Large spin-relaxation anisotropy in bilayer-graphene/WS2 heterostructures

Omar, S.; Madhushankar, B. N.; van Wees, B. J.

Published in:
Physical Review B

DOI:
10.1103/PhysRevB.100.155415

Publication date:
2019

Large spin-relaxation anisotropy in bilayer-graphene/WS_2 heterostructures

S. Omar,* B. N. Madhushankar, and B. J. van Wees
The Zernike Institute for Advanced Materials, University of Groningen, Nijenborgh 4, 9747 AG, Groningen, The Netherlands

(Received 18 June 2019; revised manuscript received 5 September 2019; published 16 October 2019)

We study spin transport in bilayer graphene (BLG), spin-orbit coupled to a tungsten di sulfide (WS_2) substrate, and measure a record spin lifetime anisotropy ~40–70, i.e., the ratio between the out-of-plane $\tau_\perp$ and in-plane spin relaxation time $\tau_{||}$. We control the injection and detection of in-plane and out-of-plane spins via the shape anisotropy of the ferromagnetic electrodes. We estimate $\tau_\perp \sim$ 1–2 ns via Hanle measurements at high perpendicular magnetic fields and via a new tool we develop: oblique spin valve measurements. Using Hanle spin-precession experiments we find a low $\tau_{||} \sim 30$ ps in the electron-doped regime which only weakly depends on the carrier density in the BLG and conductivity of the underlying WS_2, indicating proximity-induced spin-orbit coupling (SOC) in the BLG. Such high $\tau_\perp$ and spin lifetime anisotropy are clear signatures of strong spin-valley coupling for out-of-plane spins in BLG/WS_2 systems in the presence of SOC and unlock the potential of BLG/transition metal dichalcogenide heterostructures for developing future spintronic applications.

DOI: 10.1103/PhysRevB.100.155415

I. INTRODUCTION

Graphene (Gr) in contact with a transition metal dichalcogenide (TMD), having high intrinsic spin-orbit coupling (SOC), offers a unique platform where the charge transport properties in Gr are well preserved due to the weak van der Waals interaction between the two materials. However, the spin transport properties are greatly affected due to the TMD-proximity induced SOC in graphene [1–3]. At the Gr/TMD interface, the spatial inversion symmetry is broken, and the graphene sublattices having $K(K')$ valleys experience different crystal potentials and spin-orbit coupling magnitudes from the underlying TMD. The electron-spin degree of freedom and its interaction with other properties such as valley pseudospins in the presence of SOC provide access to spintronic phenomena such as spin-valley coupling [4–9], spin-Hall effect [10,11], (inverse) Rashba-Edelstein effect [12–16], and even topologically protected spin states [17–21] which are not possible to realize in pristine graphene. The mentioned effects are sought after for realizing enhancement and electric field control of SOC [1,3,22–26], efficient charge-current to spin-current conversion and vice versa [10,27–29], which will be the building blocks for developing novel spintronic applications [13,30].

Experiments on Gr/TMD systems confirm the presence of enhanced spin-orbit coupling [3,31] and the anisotropy in the in-plane ($\tau_{||}$) and out-of-plane ($\tau_\perp$) spin relaxation times [7,9,32] in single layer graphene. Recent theoretical studies [22,23] predict that due to the special band structure of bilayer graphene on a TMD substrate, it is expected to show a larger spin-relaxation anisotropy $\eta = \frac{\tau_\perp}{\tau_{||}}$ even up to 10 000 [23], which is approximately 1000 times higher than the highest reported η values for single-layer graphene-TMD heterostructures [9,33]. As explained in Ref. [23], a finite band gap opens up in bilayer graphene (BLG) in the presence of a built-in electric field at the BLG/TMD interface, which can be tuned via an external electric field. The BLG valence (conduction) band is formed via the carbon atom orbitals at the bottom (top) layer. As a consequence, due to the closer proximity of the bottom BLG layer with the TMD, the BLG valence band has almost two order higher magnitude of SOC of spin-valley coupling character than the SOC in the conduction band. This modulation in the SOC can be accessed in two ways: either by the application of a back-gate voltage by tuning the Fermi energy or via the electric field by changing the sign of the orbital gap. Depending on whether the graphene is hole or electron doped, and the magnitude of the electric field at the interface, BLG can therefore exhibit the effect of spin-valley coupling in the magnitude of spin-relaxation anisotropy ratio η.

In this paper, we report the transport of both in-plane and out-of-plane spins in BLG supported on a TMD substrate, i.e., tungsten disulfide (WS_2). We inject and detect the out-of-plane spins in graphene via a purely electrical method by exploiting the magnetic shape anisotropy of the ferromagnetic electrodes at high magnetic fields [34–36], in contrast with the optical injection of out-of-plane spins into Gr/TMD systems in Refs. [37,38]. We extract $\tau_\perp \sim$ 1 ns–2 ns, which results in $\eta = \frac{\tau_\perp}{\tau_{||}} \sim$ 40–70 via two independent methods: Hanle measurements at high perpendicular magnetic field and a newly developed tool *oblique spin valve* measurements. Such large η confirms the existence of strong spin-valley coupling for the out-of-plane spins in BLG/TMD systems. We find a weak modulation in both $\tau_{||}$ and $\tau_\perp$ as a function of charge carrier density in the electron-doped regime in the BLG. $\tau_{||}$ varies from 15–30 ps, with such short values indicating the presence of a very strong spin-orbit coupling in the BLG, induced by the WS_2 substrate.

*Corresponding author: s.omar@rug.nl

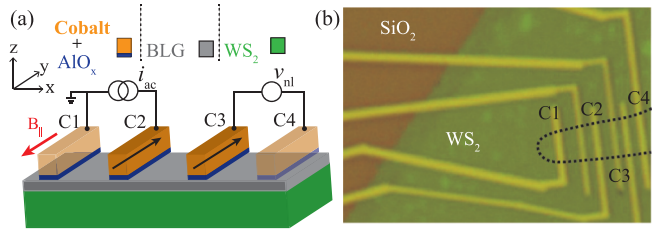

FIG. 1. (a) Nonlocal spin-transport measurement scheme. The ferromagnetic electrodes C2-C3 are premagnetized along the y axis by applying an in-plane magnetic field. The outer electrodes C1 and C4 act as reference electrodes. (b) An optical image of a part of WS_2/BLG sample (stack A) where the measurements are performed. The BLG is outlined with a black dashed line which extends further to the right.

II. DEVICE FABRICATION AND MEASUREMENTS

Bilayer-graphene/WS_2 samples are prepared on a SiO_2/Si substrate (thickness $t_{SiO_2} \sim 500$ nm) via a dry pickup transfer method [39] (see the Supplemental Material [40] for fabrication details). We study two bottom-WS_2/BLG samples (thickness $t_{WS_2} \sim 3$ nm), labeled as stack A and stack B, and present the data from the left region of stack A [Fig. 1(b)] as a representative sample, i.e., the graphene region on WS_2 not covered with the hBN flake from the top. Additional measurements from stack B and the right-side region of stack A are presented in the Supplemental Material, and they also show similar results. We use a low-frequency ac lock-in detection method to measure the charge and spin transport properties of the graphene flake. In order to measure the I-V behavior of the bottom WS_2 flake and for gate-voltage application, a Keithley 2410 dc voltage source was used. All measurements are performed at Helium temperature (4 K) under vacuum conditions in a cryostat.

Details of charge and spin-transport measurement [41–43] methods and TMD characterization are provided in the Supplemental Material. We obtain the BLG electron-mobility $\mu_e \sim 3000$ cm^2 V^{-1} s^{-1}, which is somewhat low compared to the previously reported mobility values in graphene on a TMD substrate [1,3].

We perform spin-transport measurements, using the measurement scheme shown in Fig. 1(a) and measure the nonlocal signal $R_{nl} = v_{nl}/i_{ac}$ as a function magnetic field. For in-plane spin transport, the spin signal is defined as $R_{nl}^{||} = \frac{R_{nl}^{P} - R_{nl}^{AP}}{2}$, where $R_{nl}^{AP(P)}$ is the R_{nl} measured for the (anti)parallel magnetization orientations of the injector-detector electrodes. From nonlocal spin-valve (SV) and Hanle spin-precession measurements, we obtain the spin diffusion coefficient D_s and in-plane spin-relaxation time $\tau_{||}$, and estimate the spin-relaxation length $\lambda_s^{||} = \sqrt{D_s \tau_{||}}$. A representative Hanle measurement for stack A is shown in Fig. 2(b) which is obtained by subtracting R_{nl}^{AP} from R_{nl}^{P} in Fig. 2(a). The fitting procedure is described in the Supplemental Material. Due to small magnitudes of in-plane spin signals and invasive ferromagnetic (FM) contacts ($\sim$1 kΩ), we were able to get information about the in-plane spins via Hanle measurements only for short injector-detector separation of about 1–2 μm. Since we could not access the hole-doped regime for the applied back-gate voltage in the range of +40 V to −45 V due to heavily n-doped samples, we only measure the spin transport in the electron-doped regime for both stacks. For stack A, we obtain $D_s \geqslant 0.01$ m^2 s^{-1} and $\tau_{||}$ in the range 18–34 ps, i.e., $\lambda_s^{||} \sim 0.45$–0.54 μm. For stack B, we obtain $D_s \sim 0.03$ m^2 s^{-1} and $\tau_{||}$ in the range 16–24 ps, i.e., $\lambda_s^{||} \sim 0.6$–0.7 μm. In conclusion, though for both samples we obtain reasonable charge transport properties, i.e., $D_s \sim 0.01$ m^2 s^{-1}, we obtain very low $\tau_{||}$ values. The weak modulation of $\tau_{||}$ with the back-gate voltage suggests a strong SOC induced in the BLG in contact with WS_2 [1] and the insignificant contribution of the spin-absorption mechanism for the applied back-gate voltage range in contrast with the behavior observed in Refs. [32,44,45].

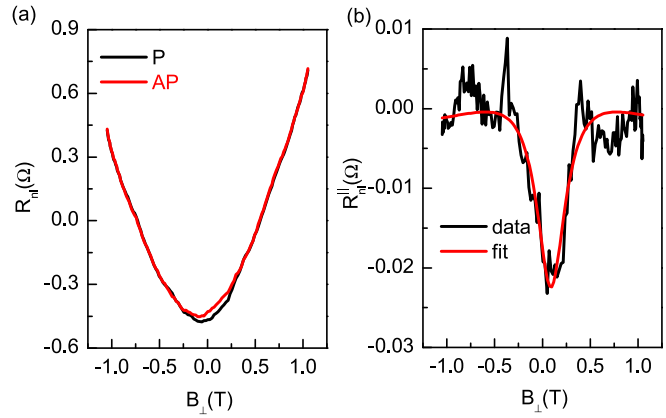

FIG. 2. (a) Parallel (P) and antiparallel (AP) Hanle curves for $L = 1$ μm ($V_{bg} = 0V$) show a strong increase in the nonlocal resistance with the applied out-of-plane magnetic field $B_\perp$, which indicates a large spin-relaxation anisotropy and the high spin-relaxation time for the out-of-plane spins. Signs of P and AP configurations are reversed because one electrode has a negative contact polarization for in-plane spins. (b) The Hanle spin signal $R_{nl}^{||}$ and the fit result in low $\tau_{||} \sim 30$ ps (stack A).

III. RESULTS AND DISCUSSION

A. Spin lifetime anisotropy: Hanle measurements

In order to explore the proposed spin-relaxation anisotropy in BLG/WS_2 systems [23], we inject out-of-plane spins electrically by controlling the magnetization direction of the FM electrodes via an external magnetic field. Due to its finite shape anisotropy along the z axis, the magnetization of the FM electrode does not stay in the device plane at high enough $B_\perp$ [46,47]. For the FM electrodes with the thickness $\sim$65 nm, their magnetization can be aligned fully in the out-of-plane direction at $B_\perp \sim 1.5$ T [5,34]. At $B_\perp \geqslant 0.3$ T, the magnetization makes an angle $\theta > 10^\circ$ with the easy axis of the FM electrode, which increases with the field (see the Supplemental Material [40] for details). In this case, the injected spins, along with the dephasing in-plane spin-signal component as shown in Fig. 2(b) also have a nonprecessing out-of-plane spin-signal component, which would increase with $B_\perp$ due to the contact magnetization aligning towards $B_\perp$ [Fig. 2(a)]. From this measurement, we can estimate $\tau_\perp$ by removing the contribution of the in-plane spin signal and the background charge (magneto)resistance, i.e., $R_{sq}(B_\perp)$ (for

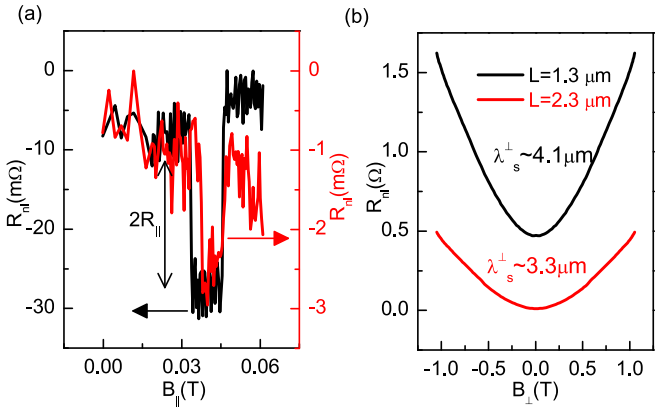

FIG. 3. (a) In-plane SV signals at the injector-detector separation $L = 1.3\ \mu$m (black) and 2.3 μm (red) with their values on the left and right axis, respectively. A background signal of 0.5 Ω (7 mΩ) which corresponds to Hanle signal at $B_\perp = 0$ T in Fig. 3(b) has been subtracted from the measured spin signal at $L = 1.3(2.3)\ \mu$m for a clear representation. (b) Measured and symmetrized Hanle curves for the same L values for the parallel configuration of FM electrodes.

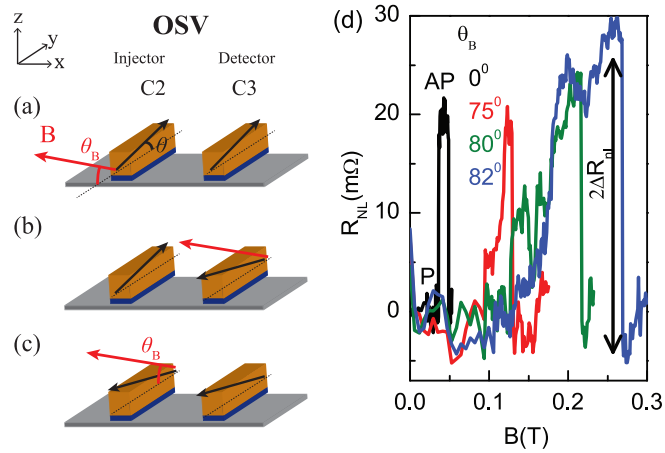

FIG. 4. (a)–(c) Steps for oblique spin-valve (OSV) measurements. The magnetization vector for the injector and detector (in black) makes an angle θ with the easy axis and the applied magnetic field B (red vector) for the magnetization reversal remains fixed at an angle θ_B throughout the measurement. The magnetization reversal for the detector and the injector are shown in (b) and (c), respectively. (d) OSV measurements at different θ_B values for the injector-detector separation $L = 1\ \mu$m. Due to the negative spin polarization of one electrode, R_{AP} is higher in magnitude than R_P. The OSV spin signal ΔR_{nl} is defined as half of the magnitude of the switch, labeled with the black arrow. The increase in the spin-valve signal magnitude at higher θ_B confirms the presence of a large spin-relaxation anisotropy. A background signal (~0.5–1 Ω) has been removed from the measured signal for a clear representation (see the Supplemental Material [40] for the original measurement).

details, refer to the Supplemental Material) and fit R_{nl} with the following equation:

$$R_{nl}(B_\perp) = \frac{P^2 R_{sq} \lambda_s^\perp e^{-\frac{L}{\lambda_s^\perp}} (\sin\theta(B_\perp))^2}{2w}. \quad (1)$$

Here $R_{nl}(B_\perp)$ is the measured signal for out-of-plane spins for the injector-detector separation L, channel width w, with out-of-plane spin relaxation length $\lambda_s^\perp$. R_{sq} is the graphene sheet resistance at $B_\perp = 0$ T. We assume that both electrodes have equal spin-injection and detection polarization P, which we obtain in the range 3–5% via regular in-plane spin-transport measurements (see the Supplemental Material [40] for details).

BLG on TMD is expected to have $\tau_\perp \gg \tau_{||}$ [23], which also implies that $R_{nl}(B_\perp)$ at $\theta = \pi/2$, i.e., $R_{nl}^\perp$ will be higher in magnitude than $R_{nl}^{||}$ at $B_\perp = 0$. In our measurements, this effect reflects as a strong increase in R_{nl} at high $B_\perp$ for both P and AP configurations [Fig. 2(a)]. Via charge magnetoresistance measurements (see the Supplemental Material [40]) for the same channel, we confirm that the observed enhancement in R_{nl} is not due to the magnetoresistance originating from the orbital effects under the applied out-of-plane magnetic field. Next, we show the distance dependence of R_{nl} in Fig. 3. The in-plane spin signal $R_{nl}^{||}$ is reduced almost by a factor of ten from 10 mΩ to 1 mΩ [Fig. 3(a)]. On the other hand, $R_{nl}(B_\perp)$ for the same distance decreases roughly by less than a factor of three for the entire range of $B_\perp$, which is evident from the ratio of $R_{nl}(B_\perp)$ in black and red curves in Fig. 3(b). From this measurement, we confirm that $\tau_\perp \gg \tau_{||}$ in the BLG/WS_2 heterostructures. We fit the experimental data in Fig. 3(b) with Eq. (1) for different L and obtain $\lambda_s^\perp \sim 3.3\ \mu$m–4.1 μm. We extract $\tau_\perp$ from the relation $\lambda_s^\perp = \sqrt{D_s \tau_\perp}$, while we assume equal D_s for in-plane and out-of-plane spins [32], and obtain $\tau_\perp \sim 1$ ns–1.6 ns, resulting in a large anisotropy $\eta \sim 50$–70.

B. Oblique spin-valve measurements

In order to confirm the spin lifetime anisotropy in the BLG/WS_2 system and to accurately measure the out-of-plane spin signals even in the possible presence of a background charge signal, we develop a new tool; *oblique spin-valve* (OSV) measurements. For the OSV measurements, we follow a similar measurement procedure as in the SV measurements. However, for the magnetization reversal of FM electrodes, we apply a magnetic field B which makes an angle θ_B with their easy axes in the y-z plane as shown in Fig. 4(a), instead of applying $B_{||}$ in SV measurements in Fig. 1(a). As a result, the magnetization of the FM electrodes also makes a finite angle θ with its easy axis. In this way, we inject and detect both in-plane and out-of-plane spins in the spin-transport channel. The in-plane magnetic field $\sim B\cos\theta_B$ is responsible for the magnetization switching of C2 and C3 (see details in the Supplemental Material). At the event of magnetization reversal at a magnetic field in the OSV measurements, the spin-signal change would appear as a sharp switch in R_{nl}. However, the magnetic field dependent background signal does not change. In this way, in the OSV measurements, we combine the advantages of both SV and the perpendicular-field Hanle measurements and obtain background-free pure spin signals. Previously reported methods [9,32] strongly rely on the fact that there is a negligible magnetic-field dependent background present with the spin signal, and the analysis is based on Hanle spin precession and dephasing. In a stark difference, the presented OSV method is based on the spin-valve

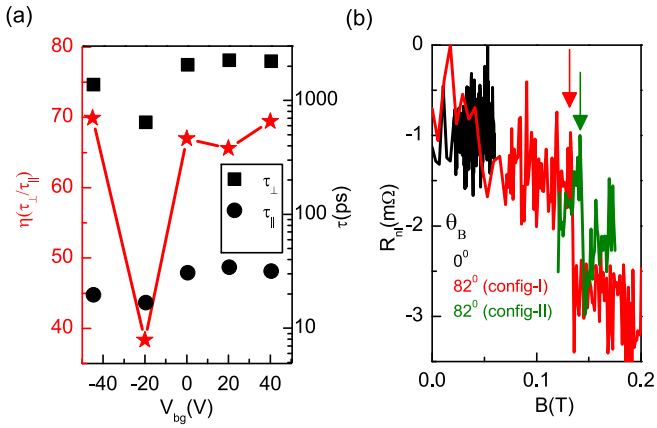

FIG. 5. (a) $\eta - V_{bg}$ plot (in red) on the left y axis and respective $\tau_{||}$ and $\tau_{\perp}$ as a function V_{bg} on the right y axis. (b) OSV measurements at $L = 4.3$ μm at $\theta_B = 0^\circ$ (black curve), $\theta_B = 82^\circ$ (config.-I) and for the swapped injector detector (config.-II) at $\theta_B = 82^\circ$. Arrows in the figure indicate the switching of electrode $C2$ in Fig. 4.

effect where we can directly probe background-free pure spin signals and study the present spin-lifetime anisotropy in such systems.

In an OSV measurement, we measure fractions of both $R_{nl}^{||}$ and $R_{nl}^{\perp}$. The OSV spin signal ΔR_{nl} consists of two components: an in-plane spin-signal component proportional to $R_{nl}^{||}\cos^2\theta$ and an out-of-plane spin-signal component proportional to $R_{nl}^{\perp}\sin^2\theta$ which get dephased by the applied magnetic field $B\sin\theta_B$ and $B\cos\theta_B$, respectively:

$$\Delta R_{nl} \simeq R_{nl}^{||}\cos^2\theta\,\zeta_{||}(B\sin\theta_B) + R_{nl}^{\perp}\sin^2\theta\,\zeta_{\perp}(B\cos\theta_B) \quad (2)$$

where $\zeta_{||(\perp)}$ is the functional form for the in-plane (out-of-plane) spin precession dynamics. At larger θ_B, the dephasing of in-plane spin signal $R_{nl}^{||}$ is enhanced. Conversely, the dephasing of out-of-plane spin signal $R_{nl}^{\perp}$ is suppressed. Also, θ increases with θ_B. Therefore, ΔR_{nl} at higher θ_B is dominated by $R_{nl}^{\perp}$ and acquires a similar form as in Eq. (1).

Due to the expected spin-lifetime anisotropy in BLG/TMD systems and as observed in Hanle measurements in Fig. 3(b), the out-of-plane spin signal magnitude increases with the magnetization angle θ. A similar effect would appear in the OSV measurements at larger θ_B values due to the fact that the magnetization switching would occur at larger θ, which would allow us to measure a larger fraction of the out-of-plane spin signal. In order to verify our hypothesis, we first measure the in-plane spin-valve signal $\Delta R_{nl} = R_{nl}^{||}$ at $\theta_B = 0^\circ$ for L $= 1$ μm, and then measure R_{nl} at different θ_B values. The measurement summary is presented in Fig. 4(d). Here, we clearly observe an increase in ΔR_{nl} up to 1.5 times with the increasing θ_B. This result is remarkable in the way that it is possible to observe such clear enhancement even with a small fraction of $R_{nl}^{\perp}$, i.e., $\propto R_{nl}^{\perp}\sin^2\theta$ contributing to ΔR_{nl}. Note that, following Eq. (2), for $\eta \leqslant 1$ (or $R_{nl}^{\perp} \leqslant R_{nl}^{||}$), we would never observe an increase in R_{nl}. Therefore the observation of an enhanced signal in the OSV measurements is the confirmation of the present large spin lifetime anisotropy in the BLG/WS_2 system.

In order to simplify the analysis and to estimate $R_{nl}^{\perp}$ from the OSV measurements, we assume that the out-of-plane signal is not significantly affected by the in-plane magnetic field component ($\sim$10 mT) at $\theta_B > 80^\circ$, and $\zeta_{\perp}(B\cos\theta_B)$ can be omitted from Eq. (2). Note that this assumption would lead to the lower bound of $R_{nl}^{\perp}$ or $\tau_{\perp}$. $R_{nl}^{||}$ and $\zeta_{||}$ are obtained via the in-plane SV and Hanle spin-precession measurements (for details refer to the Supplemental Material). From $R_{nl}^{\perp}$, we obtain $\lambda_s^{\perp} \sim 3.7$–$4$ μm, which is similar to $\lambda_s^{\perp}$ obtained via Hanle measurements and confirms the validity of the analysis. Using $\lambda_s^{\perp} = \sqrt{D_s\tau_{\perp}}$, we estimate $\tau_{\perp} \sim 1$–2 ns and the lower limit of $\eta \sim 70$ for V_{bg} between -45 V and 40 V except at $V_{bg} = -20$ V [Fig. 5(a)]. Such high magnitude of $\tau_{\perp} \sim 1$ ns is also expected theoretically even in the presence of spin-orbit coupling [23], which is comparable to the spin relaxation times observed in ultraclean graphene [5,48–50] and is a clear signature of strong spin-valley coupling present in the BLG/WS_2 system (see the Supplemental Material [40] for additional measurements).

In the presence of large η values in BLG/WS_2 heterostructures, the out-of-plane spin signal can still be detected at larger distances via OSV measurements whereas the in-plane is not even possible to detect. We present such a case in Fig. 5(b) for L $= 4.3$ μm, where no in-plane spin signal is detected. However, we clearly measure $\Delta R_{nl} = 1.5$ mΩ for $\theta_B = 82^\circ$ and obtain a similar result by swapping the injector and detector electrodes. The presented measurement unambiguously establishes the fact that indeed due to extremely large η, even though we measure a small fraction $\sim R_{nl}^{\perp}\sin^2\theta$ of $R_{nl}^{\perp}$, its magnitude is larger than the in-plane spin signal.

IV. CONCLUSIONS

In summary, we report the first spin-transport measurements on a bilayer-graphene/TMD system. We find low in-plane spin relaxation times in the range of 20–40 ps which weakly depend on the carrier density and conductivity of the underlying TMD and therefore suggest a strong proximity induced spin-orbit coupling in the BLG. Via Hanle and OSV measurements, we electrically inject and detect out-of-plane spins in the BLG/WS_2 system. We estimate the out-of-plane spin relaxation time $\sim$1–2 ns and the anisotropy value between 40 $\sim$ 70. The possible origin of lower value could have multiple reasons, such as relative crystallographic alignment of BLG and TMD lattices, which affects the valley-Zeeman type SOC, the cleanliness and interaction between the two layers, and the doping of individual layers. We do not have a direct experimental control over these parameters. It is noteworthy that obtained η and $\tau_{\perp}$ for BLG/TMD are much larger compared to previously reported values in Gr/TMD systems in Refs. [9,32]. These results confirm the theoretical prediction that the BLG/TMD systems are highly anisotropic and show efficient spin-valley coupling for out-of-plane spins. Obtained results unlock the potential of graphene/TMD systems and confirm that the spin-lifetime anisotropy is a generic phenomenon to these heterostructures which is not limited to only single-layer graphene and TMD heterostructures but extends over to bilayer-graphene and thicker TMDs. These findings would be crucial in developing future spintronic devices such as efficient spin filters and spin field-effect transistors.

ACKNOWLEDGMENTS

We acknowledge J. G. Holstein, H. H. de Vries, T. Schouten, and H. Adema for their technical assistance. We thank M. H. D. Guimarães for critically reading the manuscript. This research work was funded by the Graphene flagship core 1 and core 2 program (Grants No. 696656 and 785219), Spinoza Prize (for B.J.v.W.) by the Netherlands Organization for Scientific Research (NWO) and supported by the Zernike Institute for Advanced Materials.

[1] Z. Wang, D.-K. Ki, J. Y. Khoo, D. Mauro, H. Berger, L. S. Levitov, and A. F. Morpurgo, Phys. Rev. X **6**, 041020 (2016).

[2] M. Gmitra and J. Fabian, Phys. Rev. B **92**, 155403 (2015).

[3] S. Omar and B. J. van Wees, Phys. Rev. B **97**, 045414 (2018).

[4] D. Xiao, W. Yao, and Q. Niu, Phys. Rev. Lett. **99**, 236809 (2007).

[5] J. C. Leutenantsmeyer, J. Ingla-Aynés, J. Fabian, and B. J. van Wees, Phys. Rev. Lett. **121**, 127702 (2018).

[6] J. Xu, T. Zhu, Y. K. Luo, Y.-M. Lu, and R. K. Kawakami, Phys. Rev. Lett. **121**, 127703 (2018).

[7] S. Zihlmann, A. W. Cummings, J. H. Garcia, M. Kedves, K. Watanabe, T. Taniguchi, C. Schönenberger, and P. Makk, Phys. Rev. B **97**, 075434 (2018).

[8] A. W. Cummings, J. H. Garcia, J. Fabian, and S. Roche, Phys. Rev. Lett. **119**, 206601 (2017).

[9] T. S. Ghiasi, J. Ingla-Aynés, A. A. Kaverzin, and B. J. van Wees, Nano Lett. **17**, 7528 (2017).

[10] C. K. Safeer, J. Ingla-Aynés, F. Herling, J. H. Garcia, M. Vila, N. Ontoso, M. R. Calvo, S. Roche, L. E. Hueso, and F. Casanova, Nano Lett. **19**, 1074 (2019).

[11] J. H. Garcia, A. W. Cummings, and S. Roche, Nano Lett. **17**, 5078 (2017).

[12] Q. Song, H. Zhang, T. Su, W. Yuan, Y. Chen, W. Xing, J. Shi, J. Sun, and W. Han, Sci. Adv. **3**, e1602312 (2017).

[13] A. Soumyanarayanan, N. Reyren, A. Fert, and C. Panagopoulos, Nature (London) **539**, 509 (2016).

[14] M. Isasa, M. C. Martínez-Velarte, E. Villamor, C. Magén, L. Morellón, J. M. De Teresa, M. R. Ibarra, G. Vignale, E. V. Chulkov, E. E. Krasovskii, L. E. Hueso, and F. Casanova, Phys. Rev. B **93**, 014420 (2016).

[15] J. C. R. Sánchez, L. Vila, G. Desfonds, S. Gambarelli, J. P. Attané, J. M. De Teresa, C. Magén, and A. Fert, Nat. Commun. **4**, 2944 (2013).

[16] K. Shen, G. Vignale, and R. Raimondi, Phys. Rev. Lett. **112**, 096601 (2014).

[17] C. L. Kane and E. J. Mele, Phys. Rev. Lett. **95**, 146802 (2005).

[18] B. Yang, M.-F. Tu, J. Kim, Y. Wu, H. Wang, J. Alicea, R. Wu, M. Bockrath, and J. Shi, 2D Mater. **3**, 031012 (2016).

[19] T. Frank, P. Högl, M. Gmitra, D. Kochan, and J. Fabian, Phys. Rev. Lett. **120**, 156402 (2018).

[20] L. Du, Q. Zhang, B. Gong, M. Liao, J. Zhu, H. Yu, R. He, K. Liu, R. Yang, D. Shi, L. Gu, F. Yan, G. Zhang, and Q. Zhang, Phys. Rev. B **97**, 115445 (2018).

[21] J. O. Island, X. Cui, C. Lewandowski, J. Y. Khoo, E. M. Spanton, H. Zhou, D. Rhodes, J. C. Hone, T. Taniguchi, K. Watanabe, L. S. Levitov, M. P. Zaletel, and A. F. Young, Nature (London) **571**, 85 (2019).

[22] J. Y. Khoo, A. F. Morpurgo, and L. Levitov, Nano Lett. **17**, 7003 (2017).

[23] M. Gmitra and J. Fabian, Phys. Rev. Lett. **119**, 146401 (2017).

[24] A. M. Afzal, M. F. Khan, G. Nazir, G. Dastgeer, S. Aftab, I. Akhtar, Y. Seo, and J. Eom, Sci. Rep. **8**, 3412 (2018).

[25] P. Ye, R. Y. Yuan, X. Zhao, and Y. Guo, J. Appl. Phys. **121**, 144302 (2017).

[26] S. Omar and B. J. van Wees, Phys. Rev. B **95**, 081404(R) (2017).

[27] M. Offidani, M. Milletarì, R. Raimondi, and A. Ferreira, Phys. Rev. Lett. **119**, 196801 (2017).

[28] C. Huang, Y. D. Chong, and M. A. Cazalilla, Phys. Rev. Lett. **119**, 136804 (2017).

[29] Y. Ando and M. Shiraishi, J. Phys. Soc. Jpn. **86**, 011001 (2016).

[30] M. Gurram, S. Omar, and B. J. van Wees, 2D Mater. **5**, 032004 (2018).

[31] Z. Wang, D.-K. Ki, H. Chen, H. Berger, A. H. MacDonald, and A. F. Morpurgo, Nat. Commun. **6**, 8339 (2015).

[32] L. A. Benítez, J. F. Sierra, W. S. Torres, A. Arrighi, F. Bonell, M. V. Costache, and S. O. Valenzuela, Nat. Phys. **14**, 303 (2018).

[33] T. Zhu and R. K. Kawakami, Phys. Rev. B **97**, 144413 (2018).

[34] N. Tombros, S. Tanabe, A. Veligura, C. Józsa, M. Popinciuc, H. T. Jonkman, and B. J. van Wees, Phys. Rev. Lett. **101**, 046601 (2008).

[35] M. Popinciuc, C. Józsa, P. J. Zomer, N. Tombros, A. Veligura, H. T. Jonkman, and B. J. van Wees, Phys. Rev. B **80**, 214427 (2009).

[36] M. H. D. Guimarães, P. J. Zomer, J. Ingla-Aynés, J. C. Brant, N. Tombros, and B. J. van Wees, Phys. Rev. Lett. **113**, 086602 (2014).

[37] A. Avsar, D. Unuchek, J. Liu, O. L. Sanchez, K. Watanabe, T. Taniguchi, B. Özyilmaz, and A. Kis, ACS Nano **11**, 11678 (2017).

[38] Y. K. Luo, J. Xu, T. Zhu, G. Wu, E. J. McCormick, W. Zhan, M. R. Neupane, and R. K. Kawakami, Nano Lett. **17**, 3877 (2017).

[39] P. J. Zomer, M. H. D. Guimarães, J. C. Brant, N. Tombros, and B. J. van Wees, Appl. Phys. Lett. **105**, 013101 (2014).

[40] See Supplemental Material at http://link.aps.org/supplemental/10.1103/PhysRevB.100.155415 for the details on charge and spin-transport measurement methods, additional data on the back-gate voltage dependence of the spin-signal and spin-relaxation time, for full modeling and simulation details on the magnetization of a bar ferromagnet, and additional high-field Hanle measurements and step-wise procedure to extract out-of-plane spin-relaxation length.

[41] M. Gurram, S. Omar, S. Zihlmann, P. Makk, C. Schönenberger, and B. J. van Wees, Phys. Rev. B **93**, 115441 (2016).

[42] N. Tombros, C. Jozsa, M. Popinciuc, H. T. Jonkman, and B. J. van Wees, Nature (London) **448**, 571 (2007).

[43] T. Maassen, I. J. Vera-Marun, M. H. D. Guimarães, and B. J. van Wees, Phys. Rev. B **86**, 235408 (2012).

[44] W. Yan, O. Txoperena, R. Llopis, H. Dery, L. E. Hueso, and F. Casanova, Nat. Commun. **7**, 13372 (2016).
[45] A. Dankert and S. P. Dash, Nat. Commun. **8**, 16093 (2017).
[46] C. Kittel, *Introduction to Solid State Physics* (Wiley, New York, 2004).
[47] B. Raes, J. E. Scheerder, M. V. Costache, F. Bonell, J. F. Sierra, J. Cuppens, J. Van de Vondel, and S. O. Valenzuela, Nat. Commun. **7**, 11444 (2016).
[48] M. Gurram, S. Omar, and B. J. van Wees, Nat. Commun. **8**, 248 (2017).
[49] J. Ingla-Aynés, M. H. D. Guimarães, R. J. Meijerink, P. J. Zomer, and B. J. van Wees, Phys. Rev. B **92**, 201410(R) (2015).
[50] M. Drögeler, C. Franzen, F. Volmer, T. Pohlmann, L. Banszerus, M. Wolter, K. Watanabe, T. Taniguchi, C. Stampfer, and B. Beschoten, Nano Lett. **16**, 3533 (2016).